A Color Filter Array Based Multispectral Camera

Johannes Brauers and Til Aach

Institute of Imaging & Computer Vision
RWTH Aachen University
Templergraben 55, D-52056 Aachen
eMail: {brauers,aach}@lfb.rwth-aachen.de
URL: http://www.lfb.rwth-aachen.de

Abstract. In this paper, we introduce a new camera concept – a multispectral camera with a color filter array well-known from common RGB cameras. The proposed system provides approximately the color fidelity of a multispectral camera while featuring the compactness and – in principle – the low costs of an RGB camera. After a review of an RGB camera and a widely used interpolation algorithm we introduce the new camera type and provide a new interpolation algorithm which retains approximately the sharpness of the original multispectral image. We accomplish this by lowpass filtering of color channel differences. Comparison results for the new interpolation algorithms as well as a comparison of the multispectral and the RGB system concepts are provided.

1 Introduction

The single-chip RGB camera is today the most popular digital camera type, being available not only in form of consumer cameras and cellular phones but also in the form of professional cameras. Additionally this camera type has been established for industrial inspection purposes, where high speed operation is an important aspect. The main advantages compared to 3-chip or multispectral cameras are low costs, small overall size and – compared to multispectral cameras – the high capture speed. The latter is due to the fact that multispectral cameras, which cannot capture two spatial and one spectral domain at once, use a motor driven filter wheel or a line scanning-based approach, what prevents the acquisition of moving objects.

The main difference of a one-chip RGB camera to other camera types is a color filter array (CFA) in front of the gray level CCD or CMOS sensor for color acquisition (see Fig. 1a for a microscopic photo taken at our laboratory). This filter is also called *Bayer pattern* or *mosaic pattern* and maps three spectral sensitivities (Fig. 1b) to the spatial domain, which results in a downsampled image in each color channel. Typically the arising aliasing artefacts are reduced with a birefringent blur filter [7], which is used as an optical low pass filter.

The acquired image from the sensor is called a *raw image* and has to be postprocessed, because each pixel position contributes to only one color channel. A comprehensive overview of the postprocessing steps can be found in [16]. One of the most important steps is demosaicking, the interpolation of a one-channel raw image to a three-channel color image. Several algorithms have been developed for demosaicking; [8] gives an overview.

Against the popularity of single-chip RGB cameras, there are several drawbacks concerning the exact acquisition of colors. Since RGB cameras violate the Luther rule, i.e. the

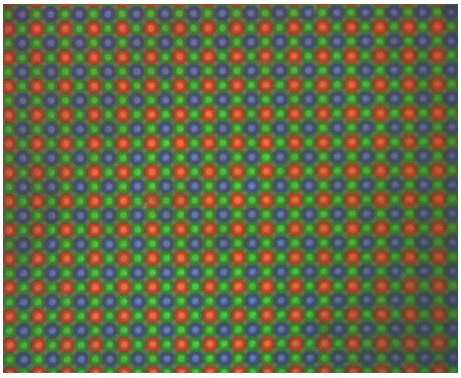

(a) Color filter array (pixel pitch: $5.6\mu m$ x $5.6\mu m$)

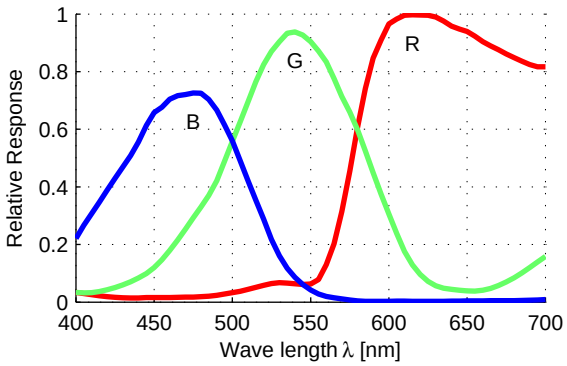

(b) Spectral sensitivities $\tau^{(R,G,B)}(\lambda)E(\lambda)$ of Sony ICX285AQ (see section 2)

Figure 1: Example of a single-chip sensor

sensor spectral sensitivies are not a linear combination of the CIE standard observer [4] ones, they lead to false colors [10]. Using multispectral technology, colorimetric acquisition, capturing of metamere colors and the correct simulation of different illuminations become possible. Users of this technology and its high color fidelity are on the one hand designers and producers of product catalogs and on the other hand companies performing industrial inspection. Multispectral cameras can be built with miscellaneous hardware. Some use a filter wheel with several spectral bandpass filters in front of the gray level sensor for capturing the spectral information [9], others use a Liquid Crystal Tuneable Filter (LCTF), where the spectral bandpass filter can be chosen by the applied voltage. However, the disadvantages of multispectral acquisition systems are their inability to capture object motion, their high costs for optical components and (depending on the type of the camera) high mechanical complexity.

We present an alternative concept to both described systems, namely a combination of a single-chip mosaicking and a multispectral camera. The new camera type approximately provides the color fidelity of a multispectral system and the simplicity of mosaicking (CFA-based) camera systems. A multispectral camera concept with a color filter array was already proposed in [2]. However, neither a comparison to a single-chip RGB system nor detailled interpolation results are provided in [2]. Furthermore, the interpolation algorithm is iterative and rather slow.

In section 2 we review the image formation process and typical pre- and postprocessing, especially demosaicking in an RGB camera. This is the basis for section 3, where we introduce the proposed system. In section 4 we compare the systems and the interpolation methods. Finally a conclusion is given in section 5.

2 RGB Demosaicking

2.1 Computation of the sensor response

In this section we review the acquisition process of a single-chip RGB camera; for the comparison of the RGB and the proposed multispectral system in section 4 we simulate

the acquisition process by using reference multispectral images. The computation of the sensor response to a certain sample is described in (1): The light source with the illuminant spectrum $S(\lambda)$ is reflected by the scene's reflectance spectrum $\beta_{x,y}(\lambda)$, filtered by the optical transmission spectrum $o(\lambda)$ and the color filter array's transmission spectrum $\tau_{x,y}^{(c)}(\lambda)$ and finally received by the sensor's relative spectral sensitivity $E(\lambda)$. We denote the spatial coordinates x, y and the filter c. $K^{(c)}$ represents the camera internal gain and the shutter setting. We assume a homogeneous illumination of the scene, so $S(\lambda)$ does not depend on the spatial coordinates x, y. Also $E(\lambda)$ is expected to be constant on the complete sensor surface and $o(\lambda)$ can be set to $o(\lambda) = 1$ (we assume an ideal optics, which does not show a wavelength-dependent behaviour). Summing over the three different color filters of the Bayer pattern, the sensor response $g_{x,y}$ is

$$g_{x,y} = \sum_{c=R,G,B} K^{(c)} \int_{\lambda_{\text{min}}}^{\lambda_{\text{max}}} S(\lambda)\, \beta_{x,y}(\lambda)\, o(\lambda)\, \tau_{x,y}^{(c)}(\lambda)\, E(\lambda)\, d\lambda. \tag{1}$$

The intermediate value $g_{x,y}$ will be distorted by an individual camera transfer function [3], which may be modeled by an offset value α, a linear factor β and a gamma value γ. Finally we obtain the sensor value $z_{x,y}$. We do not consider noise explicitly since it is implicitly included in the reference images, which we use for comparison of the RGB and proposed system. The response $z_{x,y}$ is thus given by

$$z_{x,y} = f(g_{x,y}) \qquad \text{e.g.} \quad f(x) = \alpha + \beta x^{\gamma}. \tag{2}$$

The transmission spectrum of the color filter array $\tau_{x,y}^{(c)}(\lambda)$ depends on the pixel coordinates x and y and can be described with masks (3)-(5) [1] for each channel by

$$m_{x,y}^{(R)} = \frac{(1+(-1)^x)}{2} \cdot \frac{(1+(-1)^y)}{2} = \left|\cos\left(\frac{\pi}{2}x\right)\right| \cdot \left|\cos\left(\frac{\pi}{2}y\right)\right| \tag{3}$$

$$m_{x,y}^{(G)} = \frac{(1-(-1)^{x+y})}{2} = \left|\sin\left(\frac{\pi}{2}(x+y)\right)\right| \tag{4}$$

$$m_{x,y}^{(B)} = \frac{(1-(-1)^x)}{2} \cdot \frac{(1-(-1)^y)}{2} = \left|\sin\left(\frac{\pi}{2}x\right)\right| \cdot \left|\sin\left(\frac{\pi}{2}y\right)\right|. \tag{5}$$

Then the final transmission spectra of the color filter array are

$$\tau_{x,y}^{(c)}(\lambda) = \tau^{(c)}(\lambda) m_{x,y}^{(c)}\,, \tag{6}$$

where $\tau^{(R,G,B)}(\lambda)$ represent the transmission spectra of the individual filters. Fig. 1b shows the combined relative spectral sensitivity of the sensor $E(\lambda)$ and the transmission spectra of the filters $\tau^{(R,G,B)}(\lambda)$.

With the above set of formulas we are able to compute the sensor response $z_{x,y}$ of a camera, given the reflectance spectrum $\beta_{x,y}(\lambda)$ of the scene and several intrinsic and extrinsic parameters. This makes it possible to use the same multispectral source image for the RGB mosaicking system as for the multispectral mosaicking system and permits a comparison in section 4. Actually we use a discretization of the above formulas to compute the results.

[1] We use the standard Bayer pattern RGGB here.

2.2 Preprocessing pipeline

The typical preprocessing pipeline is described in [16] and will here be only briefly discussed. After the acquisition of an image $z_{x,y}$, defective sensor pixels are corrected by using neighborhood pixel information. Then a linearization of the camera transfer function [3] takes place, which corrects a nonlinear behaviour of the sensor and the succeeding electronic processing. Furthermore the white balance is applied, which maps white objects to white color, even if they are illuminated with different light sources.

2.3 Basic demosaicking

One simple approach to perform the interpolation is bilinear interpolation, which can be expressed with linear convolution kernels. We assume $z_{x,y}$ to be the complete gray level sensor output (raw image) and $z_{x,y|c}$ the masked sensor response for color channel c defined as

$$z_{x,y|c=R} = z_{x,y} \cdot m_{x,y}^{(R)} \ . \tag{7}$$

Thus e.g., $z_{x,y|R}$ is an image where three quarters are black pixels due to the masking. Bilinear interpolation can be done by convolution with the filter kernels given by

$$H_{R,B} = H_{1,3} = \frac{1}{4}\begin{pmatrix} 1 & 2 & 1 \\ 2 & 4 & 2 \\ 1 & 2 & 1 \end{pmatrix} \qquad H_G = H_2 = \frac{1}{4}\begin{pmatrix} 0 & 1 & 0 \\ 1 & 4 & 1 \\ 0 & 1 & 0 \end{pmatrix}. \tag{8}$$

The estimated output signal then is

$$\hat{z}_{x,y}^{(c)} = z_{x,y|c} * H_c \ , \tag{9}$$

where H_c denotes the filter kernel, $z_{x,y|c}$ the masked sensor signal for the corresponding color channel c and $\hat{z}_{x,y}^{(c)}$ the estimated color plane c.

2.4 Advanced demosaicking

Interpolation according to (8) and (9) interpolates the color channels separately and does not exploit the correlation between them [15]. We will now review (in a more generic view) a demosaicking algorithm [14] which makes use of the correlation and is part of many other demosaicking algorithms (e.g. [11], [5], [12]). The algorithm exploits the correlation of color channels by building color differences between the channels – therefore either the red or blue channel is subtracted from the green one according to

$$\hat{K}_R = (\hat{G} - \hat{R})(1 - m^{(B)}) \qquad \hat{K}_B = (\hat{G} - \hat{B})(1 - m^{(R)}). \tag{10}$$

To simplify notation, we use the abbreviations $\hat{R} \equiv \hat{z}_{x,y}^{(R)}$, $\hat{G} \equiv \hat{z}_{x,y}^{(G)}$ and $\hat{B} \equiv \hat{z}_{x,y}^{(B)}$ for the interpolated color layers and $R \equiv z_{x,y|R}^{(R)}$, $G \equiv z_{x,y|G}^{(G)}$ and $B \equiv z_{x,y|B}^{(B)}$ for the measured data. Note that R, G and B are zero except for the measured data, so that $R + G + B$ results in a raw image Z.

The color difference layers $\hat{K}_R$ and $\hat{K}_B$ are also called chromatic layers, the green layer is considered as a luminance layer.

Now a smoothing operation is performed in the chromatic domain $\hat{K}_R$ and $\hat{K}_B$, which enhances the subjective image quality [14]. The convolution kernel F given by

$$F = \frac{1}{4} \begin{pmatrix} 0 & 1 & 0 \\ 1 & 0 & 1 \\ 0 & 1 & 0 \end{pmatrix} \tag{11}$$

is used for smoothing. Since all blue positions on the difference channel $\hat{K}_R$ are masked out according to (10), a correction term with factor two has to be applied as follows:

$$\bar{K}_R = (\hat{K}_R * F)m^{(R)} + 2(\hat{K}_R * F)m^{(G)} = (\hat{K}_R * F)(m^{(R)} + 2m^{(G)}) \tag{12}$$

The new smoothed channels will be denoted with a bar ($\bar{K}_R$, $\bar{K}_B$). An analog operation is performed on the blue difference channel $\hat{K}_B$ by

$$\bar{K}_B = (\hat{K}_B * F)m^{(B)} + 2(\hat{K}_B * F)m^{(G)} = (\hat{K}_B * F)(m^{(B)} + 2m^{(G)}). \tag{13}$$

The final interpolation result for the green channel is computed using original measurement values (R, G, B) and the smoothed color difference channel values $\bar{K}_R$ and $\bar{K}_B$. The computation of $\bar{R}$ and $\bar{B}$ is performed analogically. $\bar{G}$, $\bar{R}$ and $\bar{B}$ thus are

$$\bar{G} = G \ + \ R + \bar{K}_R m^{(R)} \ + \ B + \bar{K}_B m^{(B)} \tag{14}$$

$$\bar{R} = R \ + \ G - \bar{K}_R m^{(G)} \ + \ \left(\hat{G} - \bar{K}_R\right) m^{(B)} \tag{15}$$

$$\bar{B} = B \ + \ G - \bar{K}_B m^{(G)} \ + \ \left(\hat{G} - \bar{K}_B\right) m^{(R)}. \tag{16}$$

After demosaicking further postprocessing is applied, namely a color correction and an output device color transformation. We apply a color correction in section 4 since the primaries of the camera and our human eyes can be different. This is caused by the violation of the Luther rule. In practice we perform a target-based color correction with a virtual GretagMacbeth ColorChecker and a least-squares approach [6].

3 Proposed System

3.1 System Description

Our proposed sensor is shown in Fig. 2a. The gray level CCD chip in the background is covered with a multispectral color filter array, which consists of color filter blocks of the size 3x2 pixel. Alternative arrangements of the color filter array are possible and can be produced with an algorithm described in [13]. However, the proposed configuration allows to use a fast bilinear interpolation, which may be an important aspect in industrial image processing tasks, where frame rates higher than 15 frames per second are common. In Fig. 2b the corresponding spectral sensitivities of the spectral bandpass filters are shown. The colors in both figures represent the colors of the filters illuminated with a white light source.

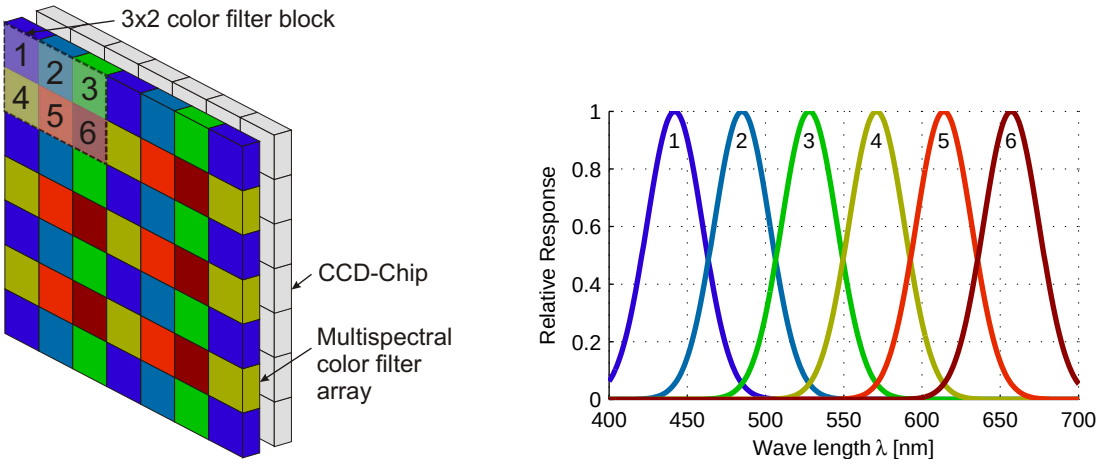

(a) Color filter array (b) Spectral sensitivities

Figure 2: Proposed color filter array

The basic principle of the camera is analogous to the RGB single-chip camera in section 2. However, the main exterior change is the number and arrangement of the color filters. Internally we now do not have a metamere but a multispectral acquisition, which means that we sample the spectrum instead of retrieving trichromatic color information. The main advantages are the possibility to detect metamere colors, i.e. spectrally dissimilar stimuli that produce the same visual/camera response [4] and to separate the illumination from the received signal.

The computation of the sensor response to a sample acquisition can be described analogously to (1) and is

$$g_{x,y} = \sum_{c=1}^{6} K^{(c)} \int_{\lambda_{\min}}^{\lambda_{\max}} S(\lambda)\, \beta_{x,y}(\lambda)\, o(\lambda)\, \tau_{x,y}^{(c)}(\lambda)\, E(\lambda)\, d\lambda\,. \tag{17}$$

The filters are described in (6), where the spectral sensitivities are taken from Fig. 2b and the mask for each spectral channel is defined by

$$m^{(c)} = \delta_{ij} \qquad \text{with } i = c-1 \text{ and } j = x \bmod 3 + 3(y \bmod 3) \qquad c \in \{1 \dots 6\}. \tag{18}$$

3.2 Basic Interpolation

A bilinear interpolation can easily be performed by

$$\hat{C}^{(c)} = C^{(c)} * H_M \tag{19}$$

with the separable filter kernel

$$H_M = \frac{1}{2}\begin{pmatrix} 1 \\ 2 \\ 1 \end{pmatrix} \cdot \frac{1}{3}\begin{pmatrix} 1 & 2 & 3 & 2 & 1 \end{pmatrix} = \begin{pmatrix} 1 & 2 & 3 & 2 & 1 \\ 2 & 4 & 6 & 4 & 2 \\ 1 & 2 & 3 & 2 & 1 \end{pmatrix} \frac{1}{6}\,. \tag{20}$$

As introduced in section 2.3, all raw image variables have no superscript marker notation (e.g. $C^{(c)}$ for the cth spectral channel) and the bilinear interpolated ones have a hat marker notation (e.g. $\hat{C}^{(c)}$). Since the masks of the spectral channels are equal except for translation, there is only one filter kernel for all channels.

3.3 Proposed Interpolation

Our proposed interpolation method makes use of spectral channel differences given by

$$\hat{K}_{ab} = m^{(b)}\hat{C}^{(a)} - C^{(b)} = \left(\hat{C}^{(a)} - C^{(b)}\right) m^{(b)}. \tag{21}$$

A raw channel $C^{(b)}$ is subtracted from a bilinear interpolated channel $\hat{C}^{(a)}$. Since the raw channel $C^{(b)}$ contains non-zero entries only on positions where real measurement data exists, a mask $m^{(b)}$ is applied.

According to the smoothing of the chromatic color difference layer in (12) and (13), we perform a bilinear interpolation in the K-domain given by

$$\bar{K}_{ab} = \hat{K}_{ab} * H_M, \tag{22}$$

which can also be interpreted as a smoothing operation. The final operation is the inverse transformation

$$\bar{C}^{(b)}m^{(a)} = \hat{C}^{(a)}m^{(a)} - \bar{K}_{ab}m^{(a)} = C^{(a)} - \bar{K}_{ab}m^{(a)}. \tag{23}$$

The masking on the left side of the equation means that only channel a will be updated.

The preceding steps have to be carried out for all channel combinations a and b. Although this seemingly is of high computional complexity, the actual complexity is quite low because of the usage of several masks.

4 Experimental Results

In this section, we present simulation results of the proposed camera system using bilinear and the proposed interpolation algorithms. Furthermore we compare the result to a common RGB system.

4.1 Test Conditions

For the tests we used multispectral images from a reference multispectral acquisition system [1] with 16 spectral channels. The images are assumed to be linearized, so we can omit the linearization. They have been resampled to six channels using the spectral sensitivities given in Fig. 2b. The RGB camera images are computed using the 16 channel multispectral images as an image source and equation (1) with the spectral sensitivities given in Fig. 1b. For a fair comparison, the resulting RGB values are transformed by applying a target based color correction. For this purpose, a virtual GretagMacbeth ColorChecker was used as a target and the linear correction matrix is computed using a least-squares regression [6]. The demosaicking of the RGB raw data is done with the differential approach [14] described in section 2.

4.2 Subjective Results

Fig. 3 shows cropped results of the *YarnPalette* image. The bilinear interpolation result of the multispectral mosaicking system in Fig. 3b produces a blurred impression and contains

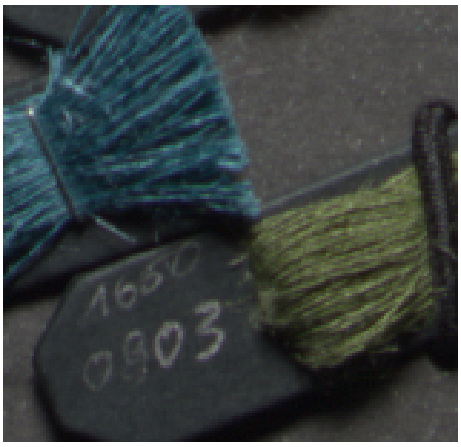

(a) Original

(b) Proposed system, bilinear interpolation

(c) Proposed system with our new interpolation algorithm

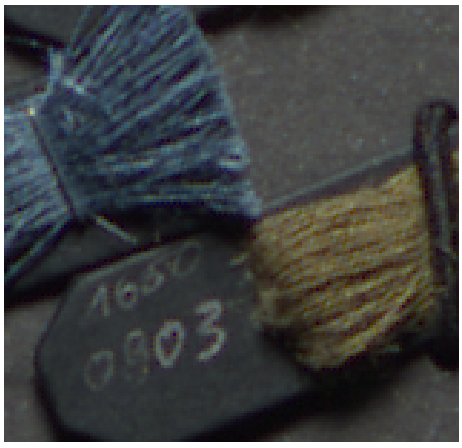

(d) RGB system

Figure 3: Detail crops of original image and simulation results (sRGB color space)

strong color fringing – the upper numbers become difficult to read. Our proposed algorithm in Fig. 3c retains the sharpness of the original better than bilinear interpolation while the color fringing is reduced. The RGB image in Fig. 3d appears to have a better spatial resolution and also less color fringing than the multispectral system, but contains strongly false colors.

4.3 Measurement Results

Objective test results are presented in table 1. The columns 2-4 show the dE_{00}-error measured in the L*a*b* color space – for computation we used a Matlab implementation suggested in [17]. $\triangle$PSNR denotes the difference *peak signal noise ratio* of the image interpolation with a bilinear and with the proposed interpolation method. It can be seen from the dE_{00} measurement that the color accuracy of a mosaicking multispectral system is higher than the one of an RGB system. Although the spatial accuracy of an RGB system is better (see Fig. 3d) the overall color performance is worse than a multispectral mosaicking system. This emphasizes a known aspect – RGB cameras produce perceptually favored

pictures, but the color accuracy is not assured.

In most cases the color fidelity of a multispectral mosaicking system can be improved with our advanced interpolation algorithm, as transpires from the dE_{00} values of the columns two and three in table 1 and from the $\triangle$PSNR values in column five. A visual assessment of the images shows that the subjective quality is greatly improved since the sharpness of the original is preserved.

Error measurement	mean dE_{00}			$\triangle$PSNR
System	Multispectral		RGB	Multispectral
Interpolation method	Bilinear	Proposed	Pei2003	Bilinear/Proposed
Artist	1.83	1.73	3.02	3.19
ColorChecker	1.61	1.73	3.36	1.77
YarnPalette	4.27	4.17	5.18	1.20
WindingCards	3.53	3.52	5.08	2.32

Table 1: Simulation results

5 Conclusion

Both a color filter array based multispectral camera and an improved interpolation algorithm have been introduced in this paper. We showed that the proposed system outperforms a common RGB system in terms of color fidelity even if the texture reproduction quality of the RGB system is slightly better. This makes the system interesting for industrial inspection purposes where spectral texture content is not as high frequent as in the presented example. The new interpolation method improves image quality and retains approximately the sharpness of original while it reduces color fringing.

Acknowledgments

The authors thank the ”Research Group Color and Image Processing“ at the RWTH Aachen (esp. Stephan Helling) and the Color AIXperts (www.color-aixperts.de) for providing high quality multispectral images.

References

[1] Color AIXperts homepage. http://www.color-aixperts.de.

[2] Gaurav A. Baone and Hairong Qi. Demosaicking methods for multispectral cameras using mosaic focal plane array technology. In Tominaga Rosen, Imai, editor, *Proceedings of SPIE Vol. 6062*, volume 6062, pages 75–87, Jan 2006.

[3] A.A. Bell, J.N. Kaftan, D. Meyer-Ebrecht, and T. Aach. An evaluation framework for the accuracy of camera transfer functions estimated from differently exposed images. In *IEEE Southwest Symposium on Image Analysis and Interpretation*, 2006.

[4] Roy S. Berns. *Billmeyer and Saltzman's Principles of Color Technology*. John Wiley & Sons Inc., 2000.

[5] Edward Chang, Shiufun Cheung, and Davis Y. Pan. Color filter array recovery using a threshold-based variable number of gradients. *IS&T/SPIE Conference on Sensors, Cameras, and Applications for Digital Photography*, 3650:p. 36–43, Mar 1999.

[6] Graham D. Finlayson and Mark S. Drew. Constrained least-squares regression in color spaces. *Journal of Electronic Imaging*, 6(4):484–493, 1997.

[7] John E. Greivenkamp. Color dependent optical prefilter for the suppression of aliasing artifacts. *Applied Optics*, 29(5):676–684, February 1990.

[8] B.K. Gunturk, J. Glotzbach, Y. Altunbasak, R.W. Schafer, and R.M. Mersereau. Demosaicking: color filter array interpolation. *IEEE Signal Processing Magazine*, 22(1):44–54, January 2005.

[9] St. Helling, E. Seidel, and W. Biehlig. Algorithms for spectral color stimulus reconstruction with a seven-channel multispectral camera. In *Proc. 2nd European Conference on Color in Graphics, Imaging and Vision CGIV 2004, Aachen, Germany, April 5-8, 2004, pp. 254-258*, 2004.

[10] F. König and Patrick G. Herzog. On the limitation of metameric imaging. *Proc. IS&T´s PICS*, 2:163–168, 1999.

[11] Xin Li and Michael T. Orchard. New edge-directed interpolation. *IEEE Transactions on Image Processing*, 10(10):1521–1527, October 2001.

[12] Rastislav Lukac, Konstantinos N. Plataniotis, Dimitrios Hatzinakos, and Marko Aleksic. A new cfa interpolation framework. In *Signal Processing*, volume 86, pages 1559–1579, 2005.

[13] Lidan Miao, Hairong Qi, and W.E. Snyder. A generic method for generating multispectral filter arrays. In *International Conference on Image Processing, 2004. ICIP '04*, volume 5, pages 3343–3346 Vol. 5, 2004.

[14] Soo-Chang Pei and Io-Kuong Tam. Effective color interpolation in CCD color filter arrays using signal correlation. *IEEE Transactions on Circuits and Systems for Video Technology*, 13(6):503–513, 2003.

[15] William K. Pratt. *Digital Image Processing: PIKS Inside*. John Wiley & Sons, Inc., New York, NY, USA, 2001.

[16] R. Ramanath, W.E. Snyder, Y. Yoo, and M.S. Drew. Color image processing pipeline. *IEEE Signal Processing Magazine*, 22(1):34–43, 2005.

[17] Gaurav Sharma, Wencheng Wu, and Edul N. Dalal. The CIEDE2000 color-difference formula: Implementation notes, supplementary test data, and mathematical observations. *Color Research and Application*, Feb 2004.